Chemico-Biological Interactions 382 (2023) 110568

Contents lists available at ScienceDirect

Chemico-Biological Interactions

journal homepage: www.elsevier.com/locate/chembioint

Research paper

Multidisciplinary docking, kinetics and X-ray crystallography studies of baicalein acting as a glycogen phosphorylase inhibitor and determination of its' potential against glioblastoma in cellular models

Rachel T. Mathomes [a,1], Symeon M. Koulas [b,1], Ioannis Tsialtas [b], George Stravodimos [b], Philip J. Welsby [c], Anna-Maria G. Psarra [b], Izabela Stasik [a], Demetres D. Leonidas [b,**], Joseph M. Hayes [a,*]

[a] School of Pharmacy & Biomedical Sciences, University of Central Lancashire, Preston, PR1 2HE, United Kingdom
[b] Department of Biochemistry & Biotechnology, University of Thessaly, Biopolis, 41500, Larissa, Greece
[c] Department of Postgraduate Medical Education, Edge Hill University, Ormskirk, L39 4QP, United Kingdom

A B S T R A C T

Glycogen phosphorylase (GP) is the rate-determining enzyme in the glycogenolysis pathway. Glioblastoma (GBM) is amongst the most aggressive cancers of the central nervous system. The role of GP and glycogen metabolism in the context of cancer cell metabolic reprogramming is recognised, so that GP inhibitors may have potential treatment benefits. Here, baicalein (5,6,7-trihydroxyflavone) is studied as a GP inhibitor, and for its effects on glycogenolysis and GBM at the cellular level. The compound is revealed as a potent GP inhibitor against human brain GPa (K_i = 32.54 μM), human liver GPa (K_i = 8.77 μM) and rabbit muscle GPb (K_i = 5.66 μM) isoforms. It is also an effective inhibitor of glycogenolysis (IC_{50} = 119.6 μM), measured in HepG2 cells. Most significantly, baicalein demonstrated anti-cancer potential through concentration- and time-dependent decrease in cell viability for three GBM cell-lines (U-251 MG, U-87 MG, T98-G) with IC_{50} values of ~20–55 μM (48- and 72-h). Its effectiveness against T98-G suggests potential against GBM with resistance to temozolomide (the first-line therapy) due to a positive O^6-methylguanine-DNA methyltransferase (MGMT) status. The solved X-ray structure of rabbit muscle GP–baicalein complex will facilitate structure-based design of GP inhibitors. Further exploration of baicalein and other GP inhibitors with different isoform specificities against GBM is suggested.

1. Introduction

Glioblastoma Multiforme (GBM) is a grade IV glioma classified by the World Health Organisation (WHO) as the most aggressive and frequently occurring primary malignancy of the central nervous system. [1] Current treatment strategies generally consist of maximal safe surgical resection prior to radiation therapy (RT) and concomitant chemotherapy with the alkylating agent temozolomide (TMZ). [2] However, despite the available treatment options, GBM remains a deadly disease with poor prognosis. In fact, there has been little improvement in the survival rates of GBM patients for more than three decades, with <5% of patients surviving 5 years and few patients surviving 2.5 years. [3] Taken together, the importance of pursuing new strategies for drug development against GBM is evident.

Glycogen phosphorylase (GP; EC 2.4.1.1), the rate-determining enzyme in the glycogenolysis pathway, is a key regulator of glucose levels and is an important therapeutic target (liver isoform) for new type 2 diabetes treatments. [4] However, it is also recently attracting significant interest for discovery of potential anti-cancer agents, including against GBM. [5–8] Metabolic reprogramming in cancer cells is a fundamental property of these cells in response to a hypoxic tumour environment. Cancer cells rely on glycolysis to cover their energy demands. Thus, reduction in glucose availability and inhibition of glycogenolysis are considered as defence mechanisms against cancer progression. [9] In this context, it was demonstrated that a GP inhibitor (CP-320626) induces apoptosis in pancreatic tumour cells by reducing glucose oxidation, nucleic acid and lipid synthesis. [10] A comprehensive *in vitro* and *in vivo* study which used U-87 GBM cells suggested GP as a promising target for new anti-cancer agents. [7] In that study, depleting liver GP was associated with glycogen accumulation and reduced cancer cell proliferation and corresponding induction of senescence, at least partially via a ROS-dependent mechanism leading to

* Corresponding author.
** Corresponding author.
E-mail addresses: ddleonidas@bio.uth.gr (D.D. Leonidas), jhayes@uclan.ac.uk (J.M. Hayes).
[1] Equal contribution.

https://doi.org/10.1016/j.cbi.2023.110568
Received 4 April 2023; Received in revised form 19 May 2023; Accepted 24 May 2023
Available online 3 June 2023

p53 activation. A very recent study demonstrated that liver glycogen phosphorylase is upregulated in GBM and inhibition of glycogen degradation sensitises GBM cells to high dose radiation. [8] Additionally, an Oncomine search (a cancer microarray database and web-based data-mining platform) revealed increased expression of liver GP in a number of tumour types [7] and it is one of 99 genes in the hypoxia metagene proposed as a hypoxic signature in head and neck squamous cell carcinomas (HNSCC) and breast cancer. [11]

Natural products including polyphenols have served as a rich source of good GP inhibitors. [12–14] This has been demonstrated by the flavonoid analogue flavopiridol (Fig. 1), which is a potent GP inhibitor with a K_i of ~1 μM (Table 1) [15] and has anti-GBM effects that may in part be attributed to its effect on GP. [16] Flavonoids have a basic chemical scaffold made up of two aromatic rings (A and B) that are linked by three carbon atoms (normally part of a heterocyclic ring that contains an oxygen, labelled C) (*c.f.* Fig. 1). The differences in ring C structural features lead to the classification of flavonoids as either flavanols, flavones, flavanones, isoflavonoids and anthocyanidins, and a number of works have studied the GP inhibitory potential of a range of these compounds, [15,17–23] the best of which are low μM inhibitors. Flavonoids including baicalein are known to bind to a variety of different enzymes, [24–27] and polypharmacology such as this can be important towards discovery of more effective agents against different conditions, such as cancer. [28] Baicalein (5,6,7-trihydroxyflavone, Fig. 1) is a flavone that was originally isolated from the roots of *Scutellaria lateriflorahas* and *Scutellaria baicalensis* (edible medicinal plants). It is a major flavonoid of *S. baicalensis* (Huangqin in Chinese), a traditional Chinese herbal medicine used in the treatment of a range of symptoms related to cancer. [29] Baicalein inhibition of GP (mainly rabbit muscle isoform) alongside a range of other flavonoids has been probed with IC_{50} values ~11–24 μM reported, [17,22] and it has demonstrated promising anti-tumour effects against a number of cancers including colon, breast, pancreatic, melanoma and esophageal squamous cell carcinoma. [30–35] It has also shown initial promise against GBM studied using the U-251 cell-line [36] and by reducing the contribution of reactive oxygen species (ROS) to invasion/migration in U-87 cells by ERK-dependent COX-2/PGE_2 activation. [37]

Biologically active GP is a dimer that has pyridoxal 5′–phosphate (PLP) as cofactor; it is regulated allosterically and by phosphorylation, with this regulation following different patterns for the three different GP isoforms (liver, muscle, brain). [38,39] There are two interconvertible GP forms, GPa and GPb. GPa is the Ser14 phosphorylated form with high activity and substrate affinity (R state); GPb is the unphosphorylated form with low activity and substrate affinity (T state). [4] A number of different GP binding sites have been reported (the catalytic, allosteric, new allosteric, inhibitor, quercetin, and glycogen storage

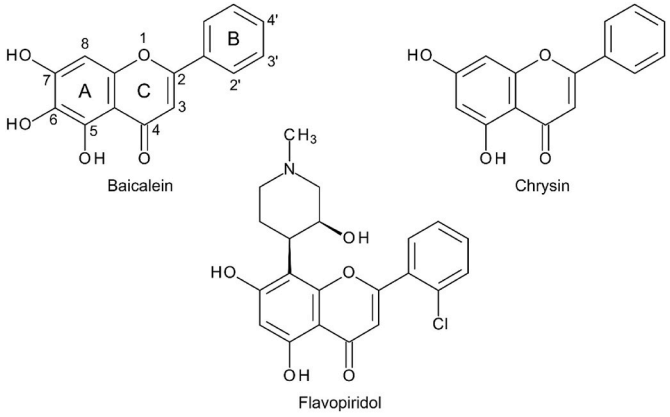

Fig. 1. Chemical structures of the flavonoids baicalein and chrysin, together with the flavonoid analogue, flavopiridol. Flavonoid atom numbering and ring labelling schemes used in text are shown for baicalein.

Table 1
Kinetics results (K_i values, μM) for baicalein against different GP isoforms in this study compared to the previously studied flavonoids, chrysin and flavopiridol. The chemical structures of the inhibitors are shown in Fig. 1.

Inhibitor	GP isoform			
	rmGPb	rmGPa	hlGPa	hbGPa
Chrysin	7.56 ± 0.81[a,c] (19.01 ± 1.85)[b,d]	5.14 ± 0.06[a,c]	7.28 ± 0.09[a,c]	–
Flavopiridol	1.24 ± 0.08[b,d]	–	–	–
Baicalein	5.66 ± 0.18[a]	–	8.77 ± 0.35[a]	32.54 ± 3.93[a]

[a] Direction of glycogen synthesis.
[b] Direction of glycogen breakdown.
[c] Reference [18].
[d] Reference [15].

sites), providing a range of options for design of structurally diverse inhibitors with therapeutic potential. The inhibitor site (also known as the caffeine binding and purine nucleoside site) is located near the entrance of the GP catalytic site, some 12 Å away. Ligands binding at the site are intercalated between the aromatic side chains of Phe285 (from the 280s loop) and Tyr613, forming sandwich complexes that exploit π – π stacking interactions as determined by X-ray crystallography. [15,18] These include the flavonoid chrysin (Fig. 1) (rmGPb: K_i = 19.01 μM in direction of glycogen breakdown; [15] K_i = 7.56 μM in direction of glycogen synthesis [18], as per Table 1) whose crystallographic binding mode (PDB code: 3EBO) is shown in Fig. 2(B), and the aforementioned flavopiridol (K_i = 1.24 μM (Table 1); PDB code: 3EBP). [15]

In this study, we report a comprehensive evaluation of baicalein as a GP inhibitor (docking, kinetics experiments against three GP isoforms and X-ray crystallography), its effects on glycogenolysis inhibition and against GBM in cellular studies. Baicalein is revealed as a potent GP inhibitor, that is effective for reduction of glycogenolysis at the cellular level. The compound demonstrated promising potential against GBM in three different cell-line models. Furthermore, the inhibitory effect of baicalein on GP activity was revealed in human hepatocarcinoma HepG2 cells. While a large number of GP structures are available (www.rcsb.org), the structure of brain GP had remained elusive until two crystal structures were recently solved: one in complex with polyethylene glycol (PEG) 400 (PDB ID: 5IKO) and another in complex with AMP (PDB ID: 5IKP). [39] We have solved and report the crystal structure of rmGP in complex with baicalein and performed a comparative structural analysis with that of brain GP.

2. Results and discussion

2.1. In silico docking

To initially assess the inhibitory potential of baicalein, Glide-SP docking calculations were employed. [40] Chrysin and its' solved crystal structure with GP (PDB code: 3EBO) was used as a benchmark for comparison (Fig. 2(B)). Conserved water molecules in protein binding sites can play a key role in bridging protein-ligand interactions. [41,42] Glide-SP docking retaining the only conserved crystallographic water molecule bridging protein-ligands contacts (ligand C4(O) with Asp283 backbone) in the GP-chrysin (PDB code: 3EBO) and GP-flavopiridol (PDB code: 3EBP) complexes led to excellent agreement between predicted and crystallographic ligand positions, with an in-place ligand RMSD (heavy atoms) of just 0.338 Å. However, redocking of chrysin using Glide-SP without any crystallographic waters retained also accurately reproduced the binding features in the crystal structure with a corresponding RMSD of 0.358 Å, without application of any constraints on the core structure to conserve the sandwich π-stacking interactions involving Phe285 and Tyr613. Glide-SP (with the conserved bridging water retained) was then used for baicalein docking (Fig. 2(A)) and produced a top-ranking pose superimposable with chrysin's

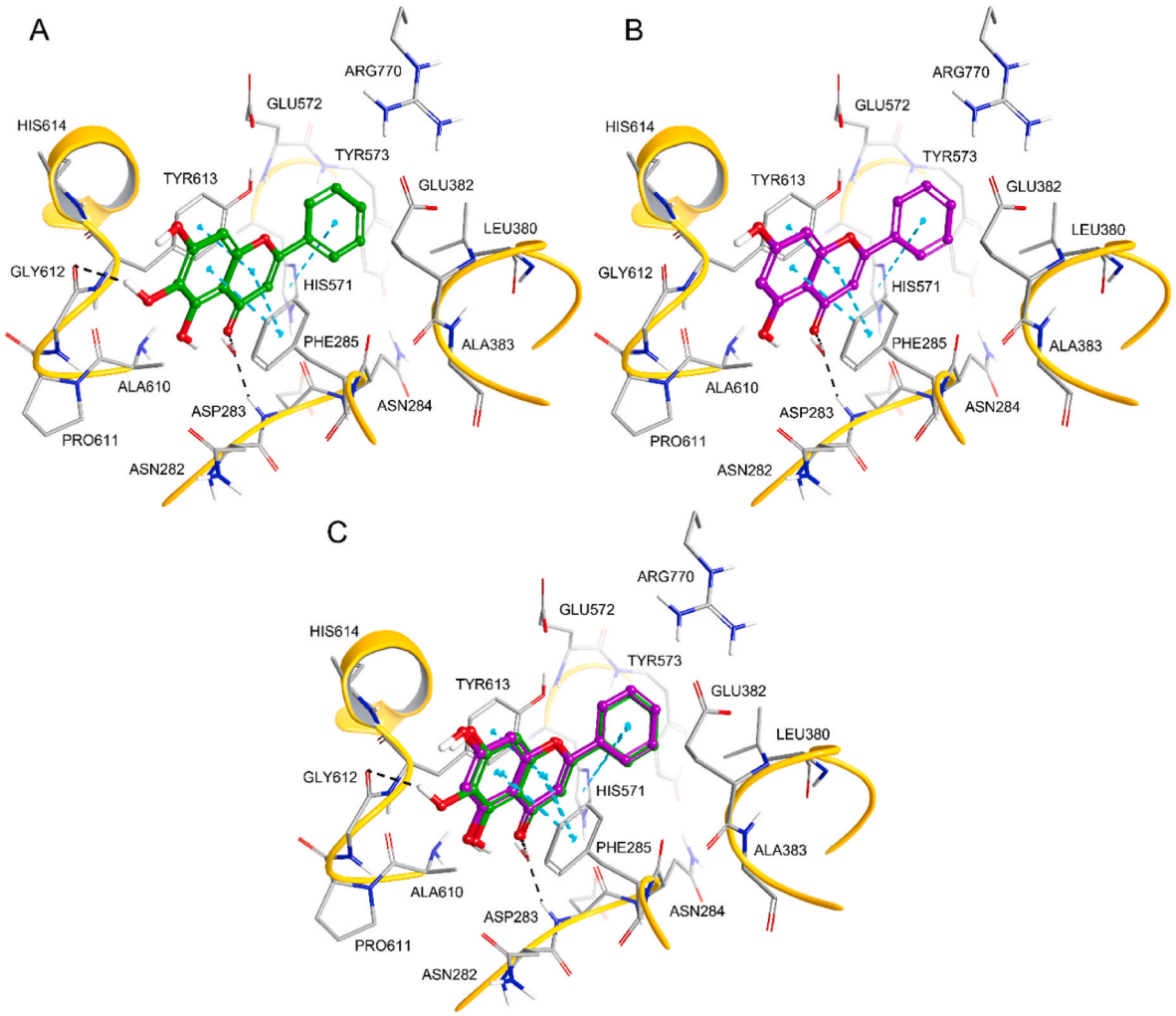

Fig. 2. Binding interactions of baicalein compared with chrysin. **(A)** top-ranked binding pose of baicalein from Glide-SP **(B)** chrysin crystallographic binding mode from PDB ID: 3EBO and **(C)** superimposition of the predicted binding pose of baicalein with the chrysin crystallographic binding mode. (Hydrogen bonds are represented by dashed black lines; π-π interactions are shown in cyan; water molecule shown was conserved in GP – chrysin (PDB code: 3EBO) and GP-flavopiridol (PDB code: 3EBP) complexes).

crystallographic position (core ring A, B and C skeletal atoms RMSD = 0.354 Å; Fig. 2(C)). Again, Glide-SP (without crystallographic waters retained) was consistent and produced a corresponding RMSD of 0.386 Å. The extra hydroxyl group of baicalein on C6 (compared to chrysin) is predicted to be involved in additional hydrogen bond interactions with the Gly612 backbone O which is ~2.5 Å away, further stabilising the predicted complex. With respect to scoring, the docking predicted baicalein (Glidescore = −8.37 and −7.92 *with* and *without* the conserved water molecule, respectively) to have similar or maybe slightly better GP inhibitory potency compared to chrysin (Glidescore = −8.31 and −7.82 *with* and *without* the conserved water molecule, respectively). Chrysin has previously reported K_i inhibition constants ranging 5.1–7.6 μM (Table 1) in the direction of glycogen synthesis for three different GP isoforms/states (rmGPa, rmGPb, hlGPa) [18].

2.2. Kinetics

Kinetic studies were performed using rabbit muscle GPb (rmGPb), human liver GPa (hlGPa), and human brain GPa (hbGPa), according to the conditions described in the Experimental section. In the brain, hbGP is predominantly found in astrocytes (which hold most of the brain glycogen stores), and to a lesser extent in neurons [43,44]. Importantly. while neurons have been reported to only express hbGP, astrocytes express both hbGP and hmGP isoforms [45]. However, as mentioned in the introduction, hlGP has been recently proposed as the important GP isoform for targeting GBM. [7,8] Hence, the relevance of K_i comparisons for different isoforms rmGPb, hlGPa and hbGPa, is the first study of this kind. The cDNA for hbGP shares 80% homology with the liver and 83% with the muscle isozymes. [46] Analysis of the Lineweaver-Burk plots for all three isoforms suggests that baicalein is a competitive inhibitor with respect to the substrate, glucose-1-phosphate (Fig. 3), which is expected for compounds binding to the inhibitor site and hinder binding of the substrate to the catalytic site while they stabilize the T-state conformation of the enzyme. [47] Baicalein was revealed as a potent low micromolar inhibitor for rmGPb (K_i = 5.66 μM) and hlGPa (K_i = 8.77 μM), with similar potency to chrysin, and determined as slightly less potent for hbGPa isoform (32.54 μM) (Table 1, Fig. 3).

2.3. X-ray crystallography

The structure of the rmGPb-baicalein was determined at 2.25 Å resolution. All atoms of the inhibitor are well defined within the electron density map (Fig. 4(A)). Baicalein binds at the inhibitor site of rmGPb in good agreement with the computational predictions (section 2.1) and does not trigger any significant conformational change to the protein structure (RMSD between the free and complexed structure 0.5 Å for

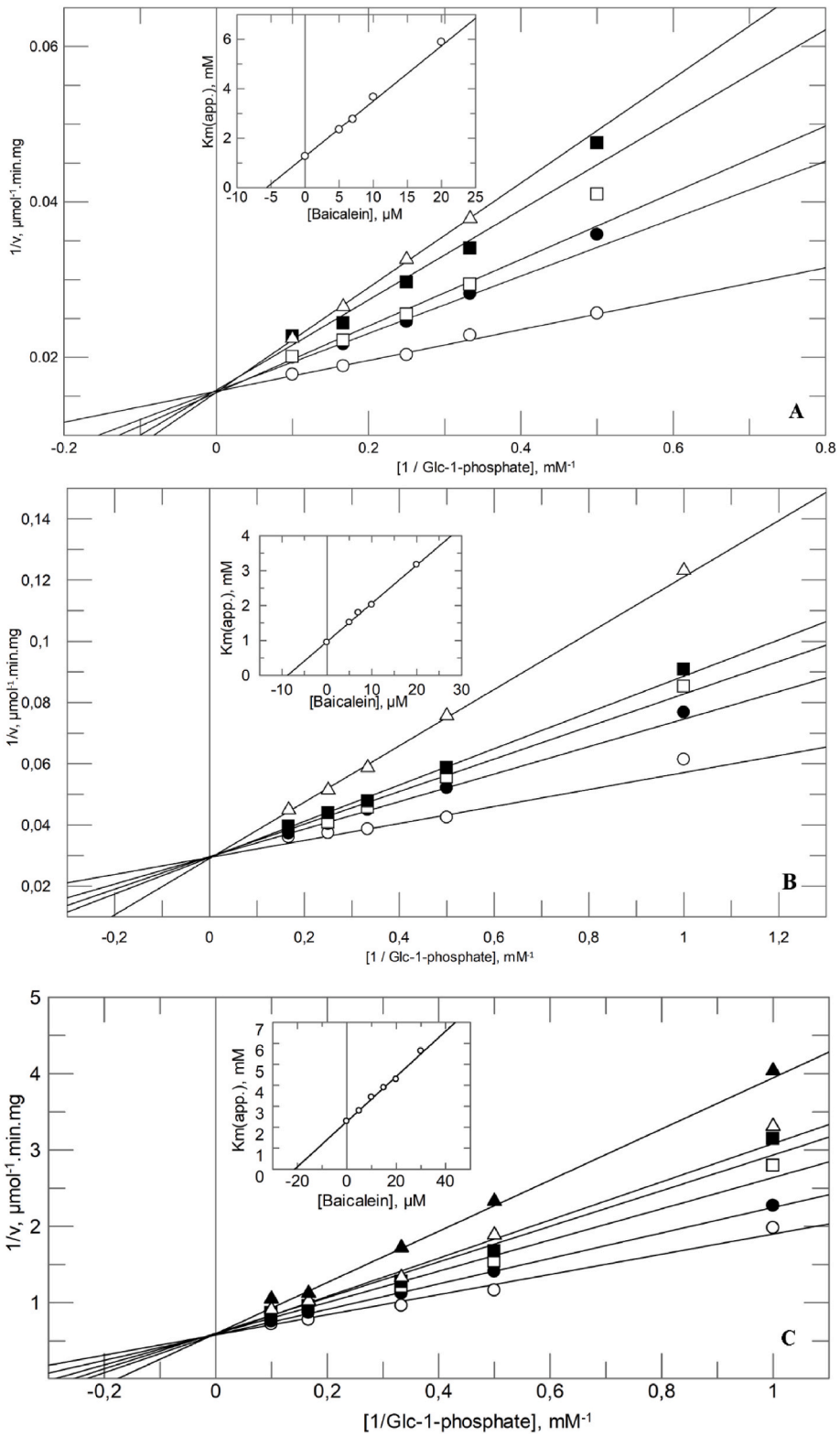

Fig. 3. Lineweaver plots for the inhibition of rmGPb (**A**), hlGPa (**B**) and hbGPa (**C**) by baicalein. Inset plots of $K_{M(app)}$ versus baicalein concentrations used to calculate the K_i values from linear regression. Baicalein concentrations used were 0 (○), 5 (●), 7 (□), 10 (■), and 20 (△) µM for rmGPB and hlGPa, and 0 (○), 5 (●), 10 (□), 15 (■), 20 (△) and 30 (▲) µM for hbGPa.

main chain atoms). Baicalein anchors at the inhibitor site by intercalating rings A and C (Fig. 1) between the aromatic side chains of Phe285 and Tyr613 (Fig. 4(B)). Hydroxyl group O3 and carbonyl oxygen of Gly612 form the only direct hydrogen bond interaction between the inhibitor and the enzyme. Two water mediated hydrogen bond interactions are also observed between carbonyl oxygen O5 of baicalein and main chain nitrogen and carbonyl oxygen of Asp283, and two between hydroxyl oxygen O4 and side chain atoms of Asn282 and Pro611.

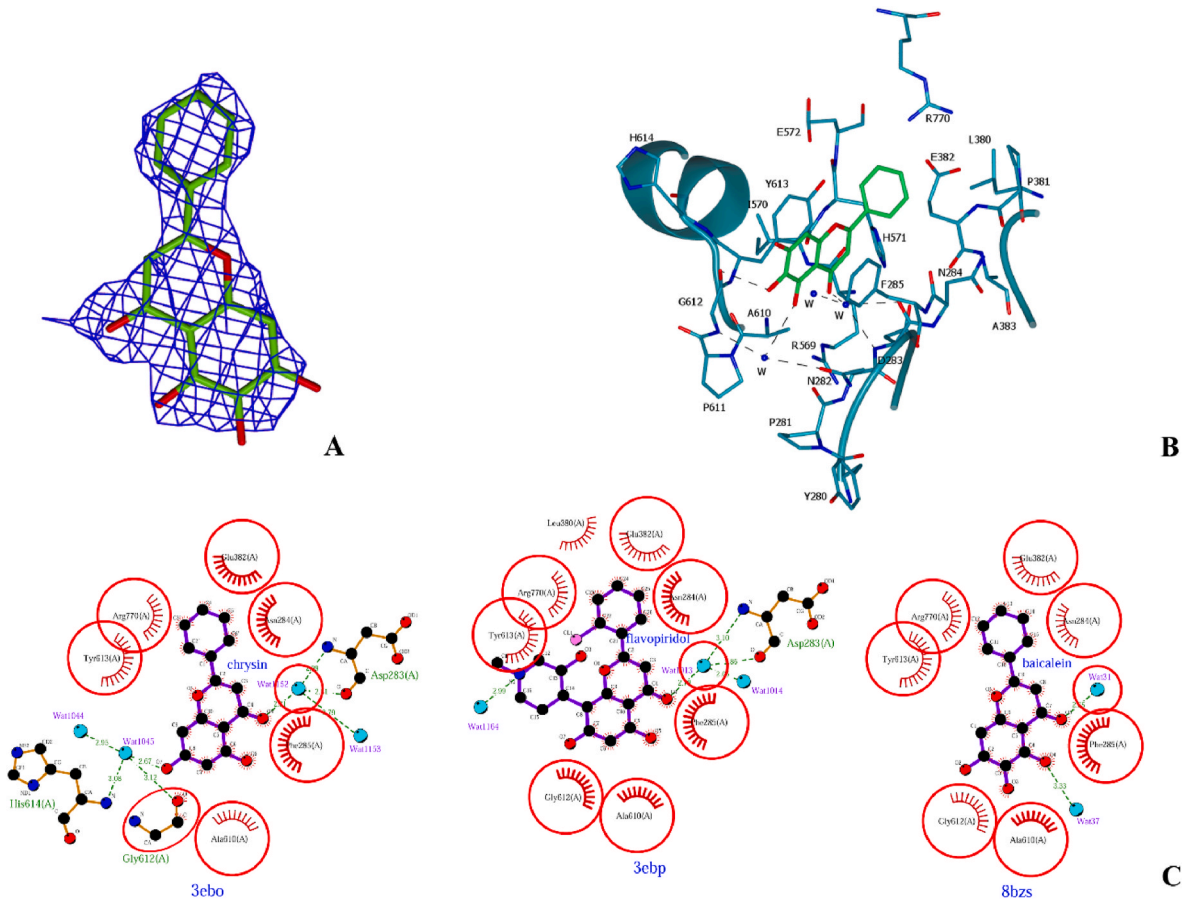

Fig. 4. (**A**) The baicalein molecule within the electron density map. (**B**) The binding of baicalein at the inhibitor site of rmGPb. Water molecules are shown as spheres and hydrogen bonds as dashed lines. (**C**) The Ligplot [48] diagrams for the GP-chrysin (PDB code: 3EBO), GP-flavopiridol (PDB code: 3EBP), and GP-baicalein (PDB code: 8BZS) complexes. The ligands and protein side chains are shown in ball-and-stick representation, with the ligand bonds coloured in purple. Hydrogen bonds are shown as green dotted lines, while the spoked arcs represent protein residues making nonbonded contacts with the ligand. The red circles and ellipses indicate protein residues that are in equivalent 3D positions when the three structural models are superposed.

2.4. Ex-vivo glycogenolysis experiments

The efficacy of baicalein to inhibit glycogen phosphorylase was assessed in human hepatocarcinoma HepG2 cells. HepG2 cells were precultured (for 24 h) in high glucose medium (25 mM glucose), in the presence of 100 nM insulin, to activate glycogen synthesis. The cells were transferred to glucose free medium, in the presence of 100 nM glucagon, conditions appropriate to induce glycogenolysis, in the absence or presence of baicalein at a concentration range of 50–500 μM. Assessment of the enzymatic activity of GP in cellular extracts of baicalein- and vehicle-treated HepG2 cells revealed high potency of baicalein to suppress GP activity, exhibiting an IC_{50} of 119.6 ± 21.4 μM (Fig. 5).

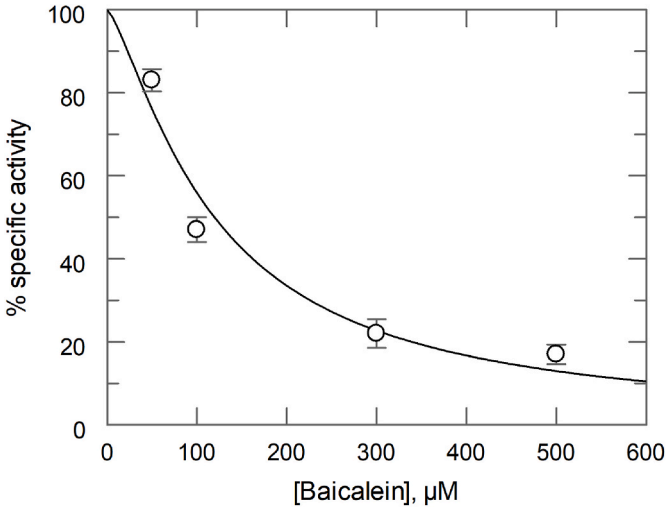

Fig. 5. GP inhibition by baicalein in HepG2 cells. GP activity was assayed in lysates of cells treated with 50, 100, 300, 500 μM baicalein for 3 h. GP activity in cells treated with DMSO (vehicle control) was used as reference condition.

2.5. Cellular glioblastoma experiments

To determine the anti-cancer potential of baicalein, the cell viability of three GBM cell lines (U-251 MG, U-87 MG, T98-G) was determined following treatment for 24, 48 and 72 h. In each case, a significant concentration- and time-dependent decrease in cell viability was observed following baicalein treatment (Fig. 6). Following 48 and 72 h of treatment, baicalein demonstrated similar efficacy in the U-251 MG cell line to that reported previously with IC_{50} values of 45.1 and 35.8 μM, respectively (Table 2). [28] In the U-87 MG cell line, efficacy increased with incubation time, demonstrated by IC_{50} values of 186 and 20.9 μM at 24 and 72 h, respectively. Perhaps the most significant result is that observed in the T98-G cell line, where treatment reduced cell viability with an IC_{50} value of approximately 50 μM at 48 and 72 h. The T98-G cell line is O^6-methylguanine-DNA methyltransferase (MGMT) positive, considered the key GBM characteristic that leads to resistance

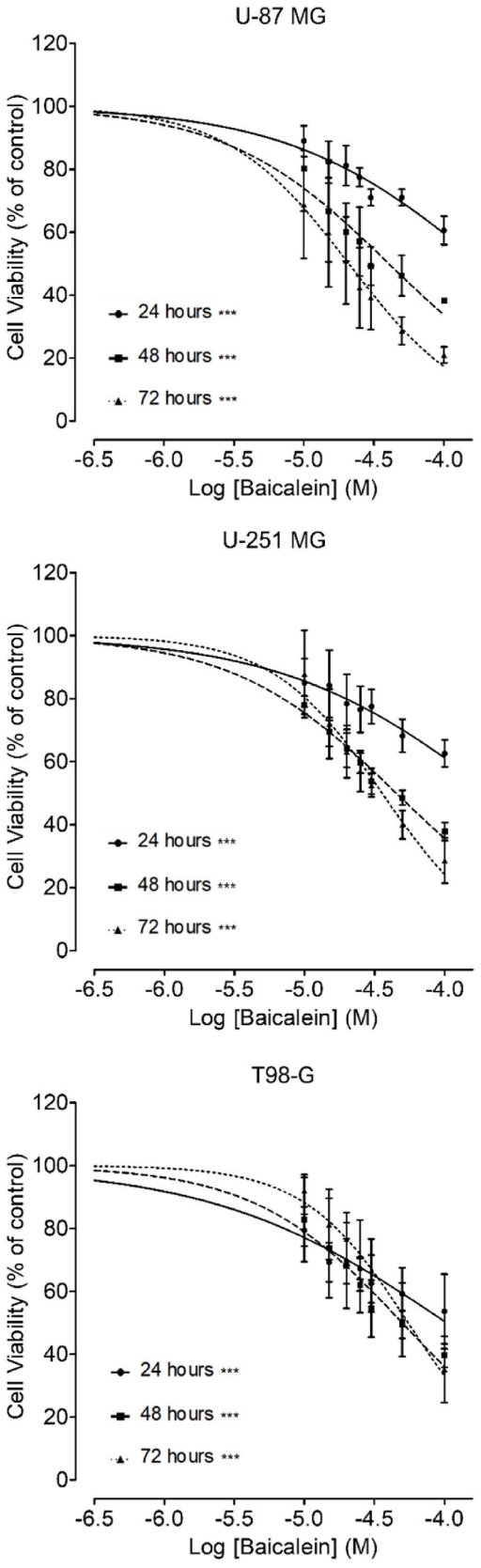

Fig. 6. Concentration and time dependent changes in cell viability of U-87 MG, T98-G, and U-251 MG cell lines following treatment with baicalein for 24, 48 and 72 h. Data represent mean ± SD of four independent experiments. Statistical significance determined by ANOVA with Bonferroni's post hoc test ($p < 0.05$).

Table 2
Cell viability IC_{50} values for the three glioblastoma cell lines, U-87 MG, T98-G, and U-251 MG, following 24, 48, and 72-h treatment with baicalein.

Cell Line	IC_{50} (μM)		
	24	48	72
U87-MG	186.3	40.4	20.9
T98G	103.6	50.0	55.1
U251-MG	220.4	45.1	35.8

to treatment with alkylating agent temozolomide, the first line therapy for the treatment of GBM. Importantly, this result suggests that baicalein could be effective in the treatment of GBM with either intrinsic or acquired resistance due to a positive MGMT status.

3. Conclusions

Discovery of drug-like GP inhibitors has potential for the development of alternative options for the treatment of GBM and other cancers. Here, we have investigated the naturally occurring flavonoid baicalein as a GP inhibitor against all three isoforms, a compound which has previously demonstrated anti-cancer potential in a number of studies. Docking studies predicted baicalein's GP inhibitory potency and binding (inhibitor site) similar to that previously reported for chrysin, and these predictions were validated by experiment. X-ray crystallography determination of the rmGPb – baicalein complex revealed binding at the inhibitor site and the interactions responsible for the observed potency. Inhibitors acting at this binding site generally act synergistically with glucose, suggesting that inhibition would decrease as normoglycaemia is achieved. [49] Baicalein was revealed as a good inhibitor of hbGPa (K_i = 32.5 μM), a low micromolar inhibitor of rmGPb and hlGPa (K_is < 10 μM) and was effective in reducing glycogenolysis (IC_{50} was 119.6 μM) in a hepatocarcinoma HepG2 cellular model, with the liver isoform suggested as the important target for GBM in recent studies. [8] In this regard, baicalein demonstrated promising potential against GBM at the cellular level, with significant reduction of cell viability in all three GBM cell-lines with low micromolar IC_{50} values identified following 72 h of treatment (20–55 μM). Further studies on baicaleins' potential against GBM are warranted, whose activity is likely to be in part due to GP inhibition. Similarly, this study also promotes further investigation of GP as a target for GBM, including the design and evaluation of isoform specific GP inhibitors (considering the different GP binding sites) against a condition that is urgently in need of new treatment approaches.

4. Experimental section

4.1. Computational details

4.1.1. Protein preparation

Exploiting the solved GPb-chrysin co-crystallised complex (PDB: 3EBO; resolution 1.9 Å), [15] the GPb receptor structure was prepared for calculations using Schrodinger's Protein Preparation Wizard. [40] Water molecules within 5 Å of het groups were initially retained, missing hydrogen atoms added, and bond orders assigned. Protonation states for acidic and basic residues were established using the PROPKA [50] predicted residue pK_a values at pH 7.0. Subsequent optimization of hydroxyl groups, histidine C/N atom flips and protonation states, and sidechain O/N atom flips of Gln and Asn residues considered hydrogen bonding patterns. Finally, the system was minimized using the OPLS3e forcefield, [51] with the RMSD of heavy atoms restrained to be within 0.3 Å of their crystallographic positions.

4.1.2. Ligand preparation

Chrysin and baicalein were prepared using Schrodinger's Maestro and LigPrep 3.9 program with Epik at a target pH of 7.0 [40]; ligands in their neutral state were selected for docking calculations.

4.1.3. Docking details

For the docking calculations with Glide 8.1, [52] the shape and properties of the GPb inhibitor site were mapped onto grids with dimensions of 24 Å × 24 Å x 24 Å centred on the native crystal structure ligand, chrysin. Default parameters were applied including van der Waals radius scaling of non-polar atoms (by 0.8). Glide docking calculations were performed in SP mode, with post-docking minimization and strain corrections applied. Docking calculations were performed without any crystallographic waters present but also retaining a conserved crystallographic water molecule in GP-chrysin (PDB code: 2EBO) and GP-flavopiridol (PDB code: 3EBP) complexes, that bridges protein-ligand contacts (ligand C4(O) with Asp283 backbone).

4.2. Kinetics measurements

rmGPb and hlGPa were produced following established protocols. [23,53] Brain GPb was produced by a modification of the Mathieu et al. protocol [54] in *E. coli* C41(DE3) bacterial cells. Bacterial cells were harvested with centrifugation and the pellet was resuspended in lysis buffer containing (50 mM Tris-HCl pH 8.0, 0.3 M NaCl, 0.1% Triton X-100, 10 mM imidazole, 1 mM PMSF and protease inhibitor cocktail). The mixture was incubated at 4 °C, for 10 min in the presence of benzonase and then sonicated at 70% amplitude, 4 °C for total 3 min. Finally, the lysate was centrifuged and the supernatant containing the soluble protein was filtered through a 0.45 μm filter and purified using IMAC (HiTrap Talon Crude, GE Healthcare) and Size Exclusion Chromatography (SEC, S200 GE Healthcare) applied on ÄKTA purifier (GE Healthcare). The chelating Sepharose resin was equilibrated with buffer A (50 mM Tris-HCl pH 8.0, 0.3 M NaCl, 0.1% Triton X-100, 10 mM imidazole) before the addition of the crude extract. The column was washed with buffer containing of 50 mM Tris-HCl pH 8, 0.3 M NaCl, 0.1% Triton X-100, 20 mM imidazole and then the protein eluted with buffer B (50 mM Tris-HCl pH 8, 0.3 M NaCl, 0.1% Triton X-100, 250 mM imidazole) followed by overnight dialysis against a buffer containing 50 mM Tris-HCl pH 8.0 and 100 mM NaCl using dialysis tubing (10 kDa MWCO, Sigma). Then, Thrombin protease (His-tagged) was added to the protein solution at 4 °C for 4 h followed by overnight dialysis against a buffer composed by 100 mM Tris/HCl pH 8.0, 50 mM 2-mercaptoethanol, and 100 mM KCl. The protein was then loaded on a SEC (S200, GE Healthcare) which was pre-equilibrated in buffer (20 mM Tris HCl pH 6.8). Thrombin protease and any uncleaved protein were removed by a HiTrap Talon Crude (GE Healthcare) column. This procedure led to 0.5 mg of pure hbGPb per litre of bacterial culture. The protein concentration was measured by absorbance measurement at 280 nm using a theoretical ε of 115170 m^{-1} cm^{-1}. The purity of the protein was assessed by SDS-PAGE analysis. Phosphorylation of hbGPb was performed using a truncated form of the γ (catalytic) subunit of rabbit skeletal muscle phosphorylase kinase as described previously [55].

Kinetic measurements were performed in the direction of glycogen synthesis as described previously [56]. rmGPb (3 μg/mL), hlGPa (1 μg/mL) or hbGPa (5 μg/mL) were assayed in a 30 mM imidazole/HCl buffer (pH 6.8) containing 60 mM KCl, 0.6 mM EDTA, and 0.6 mM DTT using constant concentrations of glycogen (0.2% w/v), AMP (1 mM for the rmGPb experiments), DMSO (2%, v/v) and various concentrations of Glc-1-P (2, 3, 4, 6 and 10 mM for rmGPb; 1, 2, 3, 4, and 6 mM for hlGPa; 0.5, 1, 2, 3, 6 and 10 mM for hbGPa). Initial velocities were calculated from the first order rate constants using the first-order rate equation and inhibition constant (K_i) values were calculated from the plot of $K_{m(app.)}$ vs [inhibitor] using the non-linear regression program GRAFIT [57] and an explicit weighting. *Ex vivo* kinetics were also performed in human HepG2 hepatocarcinoma cells as described in section 4.4.

4.3. X-ray crystallography

Ligand complex was produced by soaking preformed rmGPb crystals [56] in a solution of 7.5 mM baicalein in the crystallization media supplemented with 30% (v/v) DMSO for 5 days at 16 °C. X-ray diffraction data were collected on a Microstar Bruker rotating anode (2.7 kW/λ = 1.5414 Å) using a Mar345 image plate at room temperature. Crystal orientation, integration of reflections, inter-frame scaling, partial reflection summation, and data reduction was performed by the program iMosflm [58] while scaling and merging of intensities, was performed by Aimless [59]. Crystallographic refinement of the complex was performed by maximum-likelihood methods using REFMAC [60] and the structure of the free T state rmGPb (pdb entry 7P7D) [61] as a starting model. Crystallographic statistics are presented in Table 3.

4.4. Glycogenolysis experiments

Human hepatocarcinoma HepG2 cells was used for the assessment of the efficacy of baicalein to suppress endogenous GP activity in an *ex vivo* cell culture system. Human HepG2 hepatocarcinoma cells were provided by the American Type Cell Collection (ATTC). Cells were cultured in Dulbecco's modified Eagle medium (DMEM), supplemented with 25 mM glucose 10% Foetal Bovine Serum (FBS), 2 mM glutamine, and 50 units/ml penicillin/streptomycin (DMEM complete medium), at 37 °C in humidified atmosphere containing 5% CO_2. Evaluation of the inhibitory activity of baicalein was performed as previously described. [23] Briefly, HepG2 cells were seeded in 60 mm culture dishes at a density of 1.0 × 10^6 and cultured in DMEM complete medium. After cell attachment (16–18 h), the medium was replaced by serum-free DMEM medium containing 10 nM dexamethasone, 25 mM glucose, and 100 nM insulin, and cells were further incubated for 16–18 h to replete glycogen stores. Cells were then incubated in the absence (1:200 DMSO, vehicle control) or presence of baicalein, at a concentration range of 50–500 μM, in serum-, phenol red-, and glucose-free DMEM medium supplemented with 100 nM glucagon for 3 h. Subsequently, cells were washed in DMEM medium without phenol red, harvested, and centrifuged at 800×*g* for 5 min. Cell pellets were resuspended in 20 mM HEPES/NaOH PH 7.1, 1 mM NaF, 1 mM PMSF and 0.05% v/v Triton X-100. Then, cell lysates were sonicated followed by centrifugation at 12000×*g* at 4 °C for 15 min. GP activity was assessed in the supernatant as described above in the presence of 0.0008% (v/v) DMSO. The IC_{50} value of baicalein was calculated using the nonlinear regression program GRAFIT. [57]

Table 3
Summary of the diffraction data processing and refinement statistics for the GPb - baicalein complex. Values in parentheses are for the outermost shell.

Data Processing and collection statistics	
Resolution (Å)	2.25 (2.32-2.25)
Reflections measured	174071 (13390)
Unique reflections	45448 (3980)
R_{merge}	0.132 (0.573)
Completeness (%)	97.5 (94.7)
$< I/\sigma(I) >$	6.3 (2.3)
Multiplicity	3.8 (3.4)
$CC^{1/2}$	0.984 (0.669)
B Wilson ($Å^2$)	32.5
No of water molecules	196
No of ligand atoms	20
R (%)	15.1 (23.1)
R_{free} (%)	20.3 (28.8)
r.m.s.d. in bond lengths (Å)	0.012
r.m.s.d. in bond angles (°)	1.81
Ramachandran plot statistics	0.12% outliers, 96.89 favored
Ramachandran Z-score	−1.49 ± 0.26
Molprobity score	1.68
Average B ($Å^2$)	
Protein atoms	32.2
Water molecules	40.3
Ligand atoms	46.2
PDB entry	8BZS

4.5. Glioblastoma cell viability assays

Four independent cell viability experiments were performed on three GBM cells lines (U-87 MG, T98-G, and U-251 MG). U-251 MG cells were obtained from University of Wolverhampton and the remaining cell lines were from American Type Cell Collection. All cell lines were maintained in Eagles Minimum Essential Media (EMEM), supplemented with L-glutamine (2 mM), 1% Non-Essential Amino Acids (NEAA), 10% FBS, 1% penicillin/streptomycin. and sodium pyruvate (1 mM). Medium and additives were from Gibco. Cells were grown at 37 °C in humidified atmosphere containing 5% CO_2. Cells were seeded at a density of 1×10^3 cells/well in 96-well plates and cultured for 24 h prior to treatment with baicalein (10, 15, 20, 30, 50 and 100 μM). The concentration of DMSO in the assay did not exceed 0.4% and was not cytotoxic to cells. Cell viability was measured at 24-, 48-, and 72-h post-treatment using resazurin (Alfa Aesar) at an excitation/emission of 535/612 nm.

Author statement

R.T.M.: Investigation, Methodology, Formal Analysis, Writing- Original draft preparation, Visualization. S.M.K.: Investigation, Methodology, Formal Analysis. Writing – Original draft. I.T.: Investigation, Formal Analysis. G.S.: Investigation, Formal Analysis. P.J.W.: Formal Analysis, Visualization, Writing- Reviewing and Editing. A-M.G.P.: Formal Analysis, Methodology, Visualization, Writing- Reviewing and Editing, Supervision. I.S.: Methodology, Formal Analysis, Supervision. D.D.L.: Conceptualization, Formal Analysis, Funding acquisition, Methodology, Writing- Reviewing and Editing, Supervision, Visualization. J.M.H.: Conceptualization, Formal Analysis, Funding acquisition, Methodology, Writing- Reviewing and Editing, Supervision, Visualization.

Declaration of competing interest

The authors declare that they have no known competing financial interests or personal relationships that could have appeared to influence the work reported in this paper.

Data availability

Data will be made available on request.

Acknowledgments

R.T.M., I.S and J.M.H. gratefully acknowledge support for this research from the Sydney Driscoll Neuroscience Foundation (SDNF). Support from project “The National Research Infrastructures on integrated biology, drug screening efforts and drug target functional characterization – INSPIRED-Thessaly” (MIS 5002550) which is implemented under the Action “Reinforcement of the Research and Innovation Infrastructure” is also acknowledged, funded by the Operational Programme “Competitiveness, Entrepreneurship and Innovation” (NSRF 2014–2020) and co-financed by Greece and the European Union (European Regional Development Fund). D.D.L. would like to acknowledge Prof. Fernando Rodrigues Lima for his kind gift of the hbGPb plasmid.

References

[1] D.N. Louis, H. Ohgaki, O.D. Wiestler, W.K. Cavenee, P.C. Burger, A. Jouvet, B. W. Scheithauer, P. Kleihues, The 2007 WHO classification of tumours of the central nervous system, Acta Neuropathol. 114 (2) (2007) 97–109.

[2] A.C. Tan, D.M. Ashley, G.Y. Lopez, M. Malinzak, H.S. Friedman, M. Khasraw, Management of glioblastoma: state of the art and future directions, Ca - Cancer J. Clin. 70 (4) (2020) 299–312.

[3] A.F. Tamimi, M. Juweid, in: S. Glioblastoma De Vleeschouwer (Ed.), Epidemiology and Outcome of Glioblastoma, 2017. Brisbane (AU).

[4] N.G. Oikonomakos, Glycogen phosphorylase as a molecular target for type 2 diabetes therapy, Curr. Protein Pept. Sci. 3 (6) (2002) 561–586.

[5] C.E. Zois, A.L. Harris, Glycogen metabolism has a key role in the cancer microenvironment and provides new targets for cancer therapy, J. Molec. Med. 94 (2) (2016) 137–154.

[6] M. Curtis, H.A. Kenny, B. Ashcroft, A. Mukherjee, A. Johnson, Y.L. Zhang, Y. Helou, R. Batlle, X.J. Liu, N. Gutierrez, X. Gao, S.D. Yamada, R. Lastra, A. Montag, N. Ahsan, J.W. Locasale, A.R. Salomon, A.R. Nebreda, E. Lengyel, Fibroblasts mobilize tumor cell glycogen to promote proliferation and metastasis, Cell Metabol. 29 (1) (2019) 141–155.

[7] E. Favaro, K. Bensaad, M.G. Chong, D.A. Tennant, D.J.P. Ferguson, C. Snell, G. Steers, H. Turley, J.L. Li, U.L. Gunther, F.M. Buffa, A. McIntyre, A.L. Harris, Glucose utilization via glycogen phosphorylase sustains proliferation and prevents premature senescence in cancer cells, Cell Metabol. 16 (6) (2012) 751–764.

[8] C.E. Zois, A.M. Hendriks, S. Haider, E. Pires, E. Bridges, D. Kalamida, D. Voukantsis, B.C. Lagerholm, R.S.N. Fehrmann, W.F.A. den Dunnen, A.I. Tarasov, O. Baba, J. Morris, F.M. Buffa, J.S.O. McCullagh, M. Jalving, A.L. Harris, Liver glycogen phosphorylase is upregulated in glioblastoma and provides a metabolic vulnerability to high dose radiation, Cell Death Dis. 13 (6) (2022) 573.

[9] L. Sun, C. Suo, S.T. Li, H. Zhang, P. Gao, Metabolic reprogramming for cancer cells and their microenvironment: beyond the Warburg Effect, Biochim. Biophys. Acta Rev. Canc 1870 (1) (2018) 51–66.

[10] W.N. Lee, P. Guo, S. Lim, S. Bassilian, S.T. Lee, J. Boren, M. Cascante, V.L. Go, L. G. Boros, Metabolic sensitivity of pancreatic tumour cell apoptosis to glycogen phosphorylase inhibitor treatment, Br. J. Cancer 91 (12) (2004) 2094–2100.

[11] S.C. Winter, F.M. Buffa, P. Silva, C. Miller, H.R. Valentine, H. Turley, K.A. Shah, G. J. Cox, R.J. Corbridge, J.J. Homer, B. Musgrove, N. Slevin, P. Sloan, P. Price, C. M. West, A.L. Harris, Relation of a hypoxia metagene derived from head and neck cancer to prognosis of multiple cancers, Cancer Res. 67 (7) (2007) 3441–3449.

[12] J.M. Hayes, A.L. Kantsadi, D.D. Leonidas, Natural products and their derivatives as inhibitors of glycogen phosphorylase: potential treatment for type 2 diabetes, Phytochemistry Rev. 13 (2) (2014) 471–498.

[13] G.A. Stravodimos, B.A. Chetter, E. Kyriakis, A.L. Kantsadi, D.S. Chatzileontiadou, V.T. Skamnaki, A. Kato, J.M. Hayes, D.D. Leonidas, Phytogenic polyphenols as glycogen phosphorylase inhibitors: the potential of triterpenes and flavonoids for glycaemic control in type 2 diabetes, Curr. Med. Chem. 24 (4) (2017) 384–403.

[14] L. Somsák, K. Czifrák, M. Tóth, É. Bokor, E.D. Chrysina, K.M. Alexacou, J.M. Hayes, C. Tiraidis, E. Lazoura, D.D. Leonidas, S.E. Zographos, N.G. Oikonomakos, New inhibitors of glycogen phosphorylase as potential antidiabetic agents, Curr. Med. Chem. 15 (2008) 2933–2983.

[15] K.E. Tsitsanou, J.M. Hayes, M. Keramioti, M. Mamais, N.G. Oikonomakos, A. Kato, D.D. Leonidas, S.E. Zographos, Sourcing the affinity of flavonoids for the glycogen phosphorylase inhibitor site via crystallography, kinetics and QM/MM-PBSA binding studies: comparison of chrysin and flavopiridol, Food Chem. Toxicol. 61 (2013) 14–27.

[16] A. Cimini, M. d'Angelo, E. Benedetti, B. D'Angelo, G. Laurenti, A. Antonosante, L. Cristiano, A. Di Mambro, M. Barbarino, V. Castelli, B. Cinque, M.G. Cifone, R. Ippoliti, F. Pentimalli, A. Giordano, Flavopiridol: an old drug with new perspectives? Implication for development of new drugs, J. Cell. Physiol. 232 (2) (2017) 312–322.

[17] S. Rocha, N. Aniceto, R.C. Guedes, H.M.T. Albuquerque, V.L.M. Silva, A.M.S. Silva, M.L. Corvo, E. Fernandes, M. Freitas, An in silico and an in vitro inhibition analysis of glycogen phosphorylase by flavonoids, styrylchromones, and pyrazoles, Nutrients 14 (2) (2022) 306.

[18] B. Chetter, E. Kyriakis, D. Barr, A.G. Karra, E. Katsidou, S.M. Koulas, V. T. Skamnaki, T.J. Snape, A.M.G. Psarra, D.D. Leonidas, J.M. Hayes, Synthetic flavonoid derivatives targeting the glycogen phosphorylase inhibitor site: QM/MM-PBSA motivated synthesis of substituted 5,7-dihydroxyflavones, crystallography, in vitro kinetics and ex-vivo cellular experiments reveal novel potent inhibitors, Bioorg. Chem. 102 (2020) 104003.

[19] A.L. Kantsadi, A. Apostolou, S. Theofanous, G.A. Stravodimos, E. Kyriakis, V. A. Gorgogietas, D.S. Chatzileontiadou, K. Pegiou, V.T. Skamnaki, D. Stagos, D. Kouretas, A.M. Psarra, S.A. Haroutounian, D.D. Leonidas, Biochemical and biological assessment of the inhibitory potency of extracts from vinification byproducts of Vitis vinifera extracts against glycogen phosphorylase, Food Chem. Toxicol. 67 (2014) 35–43.

[20] A. Kato, N. Nasu, K. Takebayashi, I. Adachi, Y. Minami, F. Sanae, N. Asano, A. A. Watson, R.J. Nash, Structure-activity relationships of flavonoids as potential inhibitors of glycogen phosphorylase, J. Agric. Food Chem. 56 (12) (2008) 4469–4473.

[21] N.F. Bras, R.P.P. Neves, F.A.A. Lopes, M.A.S. Correia, A.S. Palma, S.F. Sousa, M. J. Ramos, Combined in silico and in vitro studies to identify novel antidiabetic flavonoids targeting glycogen phosphorylase, Bioorg. Chem. 108 (2021) 104552.

[22] S. Jakobs, D. Fridrich, S. Hofem, G. Pahlke, G. Eisenbrand, Natural flavonoids are potent inhibitors of glycogen phosphorylase, Mol. Nutr. Food Res. 50 (1) (2006) 52–57.

[23] C.E. Drakou, C. Gardeli, I. Tsialtas, S. Alexopoulos, A. Mallouchos, S.M. Koulas, A. S. Tsagkarakou, D. Asimakopoulos, D.D. Leonidas, A.G. Psarra, V.T. Skamnaki, Affinity crystallography reveals binding of pomegranate juice anthocyanins at the inhibitor site of glycogen phosphorylase: the contribution of a sugar moiety to potency and its implications to the binding mode, J. Agric. Food Chem. 68 (37) (2020) 10191–10199.

[24] J.D. Deschamps, V.A. Kenyon, T.R. Holman, Baicalein is a potent in vitro inhibitor against both reticulocyte 15-human and platelet 12-human lipoxygenases, Bioorg. Med. Chem. 14 (12) (2006) 4295–4301.

[25] H. Zhang, J. Zhai, L.P. Zhang, C.Y. Li, Y.N. Zhao, Y.Y. Chen, Q. Li, X.P. Hu, In vitro inhibition of glyoxalase I by flavonoids: new insights from crystallographic analysis, Curr. Top. Med. Chem. 16 (4) (2016) 460–466.
[26] K.S. Oh, B.K. Oh, C.H. Park, J. Mun, S.H. Won, B.H. Lee, Baicalein potently inhibits rho kinase activity and suppresses actin stress fiber formation in angiotensin II-stimulated H9c2 cells, Biol. Pharm. Bull. 35 (8) (2012) 1281–1286.
[27] Y.J. Teng, H. Nian, H.T. Zhao, P. Chen, G. Wang, Biotransformation of baicalin to baicalein significantly strengthens the inhibition potential towards UDP-glucuronosyltransferases (UGTs) isoforms, Pharmazie 68 (9) (2013) 763–767.
[28] A.A. Antolin, P. Workman, J. Mestres, B. Al-Lazikani, Polypharmacology in precision oncology: current applications and future prospects, Curr. Pharmaceut. Des. 22 (46) (2016) 6935–6945.
[29] C.S. Cheng, J. Chen, H.Y. Tan, N. Wang, Z. Chen, Y. Feng, Scutellaria baicalensis and cancer treatment: recent progress and perspectives in biomedical and clinical studies, Am. J. Chin. Med. 46 (1) (2018) 25–54.
[30] L. Huang, B. Peng, Y. Nayak, C. Wang, F.S. Si, X. Liu, J. Dou, H.X. Xu, G.Y. Peng, Baicalein and baicalin promote melanoma apoptosis and senescence via metabolic inhibition, Front. Cell Dev. Biol. 8 (2020) 836.
[31] M.Q. Su, Y.R. Zhou, X. Rao, H. Yang, X.H. Zhuang, X.J. Ke, G.Y. Peng, C.L. Zhou, B. Y. Shen, J. Dou, Baicalein induces the apoptosis of HCT116 human colon cancer cells via the upregulation of DEPP/Gadd45a and activation of MAPKs, Int. J. Oncol. 53 (2) (2018) 750–760.
[32] H. Takahashi, M.C. Chen, H. Pham, E. Angst, J.C. King, J. Park, E.Y. Brovman, H. Ishiguro, D.M. Harris, H.A. Reber, O.J. Hines, A.S. Gukovskaya, V.L.W. Go, G. Eibl, Baicalein, a component of Scutellaria baicalensis, induces apoptosis by Mcl-1 down-regulation in human pancreatic cancer cells, Bba-Mol. Cell Res. 1813 (8) (2011) 1465–1474.
[33] H.B. Zhang, P. Lu, Q.Y. Guo, Z.H. Zhang, X.Y. Meng, Baicalein induces apoptosis in esophageal squamous cell carcinoma cells through modulation of the PI3K/Akt pathway, Oncol. Lett. 5 (2) (2013) 722–728.
[34] H. Chung, H.S. Choi, E.K. Seo, D.H. Kang, E.S. Oh, Baicalin and baicalein inhibit transforming growth factor-beta 1-mediated epithelial-mesenchymal transition in human breast epithelial cells, Biochem. Bioph. Res. Commun. 458 (3) (2015) 707–713.
[35] Y. Gao, S.A. Snyder, J.N. Smith, Y.C. Chen, Anticancer properties of baicalein: a review, Med. Chem. Res. 25 (8) (2016) 1515–1523.
[36] G.L. Jiang, L. Zhang, J.K. Wang, H.J. Zhou, Baicalein induces the apoptosis of U251 glioblastoma cell lines via the NF-kB-p65-mediated mechanism, Anim. Cell Syst. 20 (5) (2016) 296–302.
[37] W.T. Chiu, S.C. Shen, J.M. Chow, C.W. Lin, L.T. Shia, Y.C. Chen, Contribution of reactive oxygen species to migration/invasion of human glioblastoma cells U87 via ERK-dependent COX-2/PGE(2) activation, Neurobiol. Dis. 37 (1) (2010) 118–129.
[38] L.F. Obel, M.S. Muller, A.B. Walls, H.M. Sickmann, L.K. Bak, H.S. Waagepetersen, A. Schousboe, Brain glycogen-new perspectives on its metabolic function and regulation at the subcellular level, Front. Neuroenergetics 4 (2012) 3.
[39] C. Mathieu, J.M. Dupret, F.R. Lima, The structure of brain glycogen phosphorylase-from allosteric regulation mechanisms to clinical perspectives, FEBS J. 284 (4) (2017) 546–554.
[40] Schrödinger Software Suite 2018-4, LLC, New York, NY, 2018..
[41] J.M. Hayes, V.T. Skamnaki, G. Archontis, C. Lamprakis, J. Sarrou, N. Bischler, A. L. Skaltsounis, S.E. Zographos, N.G. Oikonomakos, Kinetics, in silico docking, molecular dynamics, and MM-GBSA binding studies on prototype indirubins, KT5720, and staurosporine as phosphorylase kinase ATP-binding site inhibitors: the role of water molecules examined, Proteins: Struct., Funct., Bioinf. 79 (3) (2011) 703–719.
[42] A.T. Garcia-Sosa, Hydration properties of ligands and drugs in protein binding sites: tightly-bound, bridging water molecules and their effects and consequences on molecular design strategies, J. Chem. Inf. Model. 53 (6) (2013) 1388–1405.
[43] A.M. Cataldo, R.D. Broadwell, Cytochemical identification of cerebral glycogen and glucose-6-phosphatase activity under normal and experimental conditions .2. Choroid-plexus and ependymal epithelia, endothelia and pericytes, J. Neurocytol. 15 (4) (1986) 511–524.
[44] I. Saez, J. Duran, C. Sinadinos, A. Beltran, O. Yanes, M.F. Tevy, C. Martinez-Pons, M. Milan, J.J. Guinovart, Neurons have an active glycogen metabolism that contributes to tolerance to hypoxia, J. Cerebr. Blood Flow Metab. 34 (6) (2014) 945–955.
[45] B. Pfeiffer-Guglielmi, B. Fleckenstein, G. Jung, B. Hamprecht, Immunocytochemical localization of glycogen phosphorylase isozymes in rat nervous tissues by using isozyme-specific antibodies, J. Neurochem. 85 (1) (2003) 73–81.
[46] A.M. Brown, B.R. Ransom, Astrocyte glycogen and brain energy metabolism, Glia 55 (12) (2007) 1263–1271.
[47] P.J. Kasvinsky, S. Shechosky, R.J. Fletterick, Synergistic regulation of phosphorylase a by glucose and caffeine, J. Biol. Chem. 253 (24) (1978) 9102–9106.
[48] R.A. Laskowski, M.B. Swindells, LigPlot+: multiple ligand-protein interaction diagrams for drug discovery, J. Chem. Inf. Model. 51 (10) (2011) 2778–2786.
[49] N.G. Oikonomakos, L. Somsak, Advances in glycogen phosphorylase inhibitor design, Curr. Opin. Invest. Drugs 9 (4) (2008) 379–395.
[50] C.R. Sondergaard, M.H.M. Olsson, M. Rostkowski, J.H. Jensen, Improved treatment of ligands and coupling effects in empirical calculation and rationalization of pK(a) values, J. Chem. Theor. Comput. 7 (7) (2011) 2284–2295.
[51] G.A. Kaminski, R.A. Friesner, J. Tirado-Rives, W.L. Jorgensen, Evaluation and reparametrization of the OPLS-AA force field for proteins via comparison with accurate quantum chemical calculations on peptides, J. Phys. Chem. B 105 (28) (2001) 6474–6487.
[52] Glide Version 8.1, Schrödinger, LLC, New York, NY, 2018.
[53] E. Kyriakis, T.G.A. Solovou, S. Kun, K. Czifrak, B. Szocs, L. Juhasz, E. Bokor, G. A. Stravodimos, A.L. Kantsadi, D.S.M. Chatzileontiadou, V.T. Skamnaki, L. Somsak, D.D. Leonidas, Probing the beta-pocket of the active site of human liver glycogen phosphorylase with 3-(C-beta-D-glucopyranosyl)-5-(4-substituted-phenyl)-1, 2, 4-triazole inhibitors, Bioorg. Chem. 77 (2018) 485–493.
[54] C. Mathieu, I.L. de la Sierra-Gallay, R. Duval, X. Xu, A. Cocaign, T. Leger, G. Woffendin, J.M. Camadro, C. Etchebest, A. Haouz, J.M. Dupret, F. Rodrigues-Lima, Insights into Brain Glycogen Metabolism: the structure of human brain glycogen phosphorylase, J. Biol. Chem. 291 (35) (2016) 18072–18083.
[55] A.L. Kantsadi, E. Bokor, S. Kun, G.A. Stravodimos, D.S.M. Chatzileontiadou, D. D. Leonidas, E. Juhasz-Toth, A. Szakacs, G. Batta, T. Docsa, P. Gergely, L. Somsak, Synthetic, enzyme kinetic, and protein crystallographic studies of C-beta-d-glucopyranosyl pyrroles and imidazoles reveal and explain low nanomolar inhibition of human liver glycogen phosphorylase, Eur. J. Med. Chem. 123 (2016) 737–745.
[56] T. Fischer, S.M. Koulas, A.S. Tsagkarakou, E. Kyriakis, G.A. Stravodimos, V. T. Skamnaki, P.G.V. Liggri, S.E. Zographos, R. Riedl, D.D. Leonidas, High consistency of structure-based design and X-ray crystallography: design, synthesis, kinetic evaluation and crystallographic binding mode determination of biphenyl-N-acyl-beta-D-glucopyranosylamines as glycogen phosphorylase inhibitors, Molecules 24 (7) (2019) 1322.
[57] R.J. Leatherbarrow, GraFit Version 6.0, Erithakus Software, Staines, UK, 2007.
[58] T.G. Battye, L. Kontogiannis, O. Johnson, H.R. Powell, A.G. Leslie, iMOSFLM: a new graphical interface for diffraction-image processing with MOSFLM, Acta Crystallogr. D Biol. Crystallogr. 67 (Pt 4) (2011) 271–281.
[59] M.D. Winn, C.C. Ballard, K.D. Cowtan, E.J. Dodson, P. Emsley, P.R. Evans, R. M. Keegan, E.B. Krissinel, A.G. Leslie, A. McCoy, S.J. McNicholas, G.N. Murshudov, N.S. Pannu, E.A. Potterton, H.R. Powell, R.J. Read, A. Vagin, K.S. Wilson, Overview of the CCP4 suite and current developments, Acta Crystallogr. D Biol. Crystallogr. 67 (Pt 4) (2011) 235–242.
[60] G.N. Murshudov, P. Skubak, A.A. Lebedev, N.S. Pannu, R.A. Steiner, R.A. Nicholls, M.D. Winn, F. Long, A.A. Vagin, REFMAC5 for the refinement of macromolecular crystal structures, Acta Crystallogr. D Biol. Crystallogr. 67 (Pt 4) (2011) 355–367.
[61] D.D. Leonidas, S.E. Zographos, K.E. Tsitsanou, V.T. Skamnaki, G. Stravodimos, E. Kyriakis, Glycogen phosphorylase revisited: extending the resolution of the R- and T-state structures of the free enzyme and in complex with allosteric activators, Acta Crystallogr. F77 (9) (2021) 303–311.